Supplementary Information for

Synergy between Dynamic Covalent Boronic Ester and Boron-Nitrogen Coordination: Strategy for Self-Healing Polyurethane Elastomers at Room Temperature with Unprecedented Mechanical Properties

Kai Song[a], Wujin Ye[a], Xingchen Gao[a], Huagao Fang[a, b], Yaqiong Zhang[c], Qi Zhang[d], Xueliang Li[e], Shanzhong Yang[a, b], Haibing Wei*[a,b], Yunsheng Ding*[a,b]*

[a]*Department of Polymer Science and Engineering, School of Chemistry and Chemical Engineering, Hefei University of Technology, Hefei, Anhui 230009, China.*
[b]*Anhui Province Key Laboratory of Advanced Functional Materials and Devices, Hefei, Anhui 230009, China.*
[c]*Biomass Molecular Engineering Center, School of Forestry and Landscape Architecture, Anhui Agricultural University, Hefei, Anhui 230036, China.*
[d]*Anhui Province Key Lab of Aerospace Structural Parts Forming Technology and Equipment, Institute of Industry & Equipment Technology, Hefei University of Technology, Hefei, Anhui 230009, China.*
[e]*Anhui Province Key Laboratory of Advanced Catalytic Materials and Reaction Engineering, School of Chemistry and Chemical Engineering, Hefei University of Technology, Hefei, Anhui 230009, China.*

Corresponding Authors: Huagao Fang; Yunsheng Ding; Haibing Wei

*Email address: fanghg@hfut.edu.cn; dingys@hfut.edu.cn; hbwei@hfut.edu.cn.

1. Materials.

Isophorone diisocyanate (IPDI) was purchased from BASF, and used as supplied without further purification. Polytetramethylene ether glycol (PTMEG, M.W.=1000), was purchased from Shanxi Sanwei Co., Ltd and dried under vacuum at 110°C for 2h before use. N-(3-dimethylaminopropyl)-N, N-diisopropanolamine (DPA) was purchased from Micxy Reagent and dried over 4Å molecular sieves. 1, 4-butanediol (BDO, 99.5%), 1, 4-phenylenebisboronic acid (98%) and 1, 2, 6-hexanetriol (98%) were purchased from Energy Chemical. Dibutyltin dilaurate (DBTDL, 95%), calcium hydride (98.5%) and deuterated solvents for NMR analysis were purchased from Aladdin. n-Hexane was purchased from Chinasun Specialty Products Co., Ltd and dried

by refluxing with calcium hydride. Tetrahydrofuran (THF) and dimethylacetamide (DMAc) were purchased from Richjoint and dried by refluxing with calcium hydride. Magnesium sulphate ($MgSO_4$, 98%) was purchased from Sinopharm Chemical Reagent.

2. Sample Preparation

2.1 Synthesis of 2,2'-(1,4-phenylene)-bis[4-(4-hydroxybutyl)-1,3,2-dioxaborolane] (HDB).

Dihydroxyl-bearing boronic ester chain extender was prepared by reacting 1, 4-phenylenediboronic acid with 1, 2, 6-hexanetriol (**Fig. S1**). Typically, 4.15 g (25mmol) of 1,4-phenylenediboronic acid and 7.37g (55mmol) of 1,2,6-hexanetriol were dissolved in 50 mL anhydrous tetrahydrofuran, into which 10.0 g of magnesium sulfate was added. The reaction system was stirred at room temperature for 24 h, followed by filtration and concentration. After solvent removal under reduced pressure, the residue was precipitated in n-hexane to yield the target compound (8.3g, 91.7%). The product was characterized by ^{1}H NMR, ^{13}C NMR and ^{11}B NMR spectroscopies. ^{1}H NMR ($CDCl_3$, 400 MHz), δ 7.78 (s, 4H), 4.55 (m, 2H), 4.40 (t, $J_1 = J_2 = 6$ Hz, 2H), 3.92 (t, $J_1 = J_2 = 6$ Hz, 2H), 3.63 (t, $J_1 = 4$ Hz, 4H), 1.72 (m, 2H), 1.60 (m, 8H), 1.45 ppm (m, 2H). ^{13}C ($CDCl_3$, 100MHz): δ 134.0, 77.5, 71.1, 62.5, 35.8, 32.4, and 21.3 ppm. Carbon adjacent to boron is not detected due to quadrupolar relaxation. ^{11}B (CDCl3, 128MHz), δ 30.0 ppm.

2.2 Synthesis of the supramolecular polyurethane elastomers (SPUEs).

The formulation of PU-B_0, PU-B_9 and PU-BN_x are presented in **Table S1**. The molar ratio of isocyanate groups with respect to hydroxyl groups was maintained at 1.0. The samples were synthesized according to **Fig. S2**. The synthesis procedure of PU-BN_x was illustrated as follows by taking PU-BN_7 as an example. Firstly, a stoichiometric mixture of IPDI (2.67 g, 12.00 mmol), dehydrated PTMEG1000 (6.00 g, 6.00 mmol)

were added into a 100 mL four-necked round-bottom glass reactor equipped with a mechanical stirrer, nitrogen inlet, and condenser with drying tube. The mixture was reacted for 2 h at 80 °C to get a linear and NCO groups terminated oligomer. After that, a predetermined amount of HDB (0.72 g, 2.00 mmol) and appropriate amount of DBTDL were dropped into the reaction mixture to extend the intermediated products. After reacting for another 2h, N-(3-dimethylaminopropyl)-N, N-diisopropanolamine (DPA) (0.87 g, 4.00 mmol) was added into the system and reacted for another 2h to get the target PU-BN_7 solution. During the chain extending process, an appropriate amount of anhydrous DMAc was added to reduce the viscosity of the reaction mixture. The PU-BN_7 films with a thickness about approximately 1.0 mm were prepared. In detail, a predetermined amount of PU-BN_7 solution was poured into the horizontally placed and freshly cleaned polytetrafluoroethylene (PTFE) mold. After drying at 80 ^{o}C for 48h, the majority of DMAc evaporated. The polymers were further dried under vacuum (80 ^{o}C) for 48h to obtain films. The sample films were stored in a silica-gel-containing desiccator at 25±1^{o}C before use.

3. Methods

3.1 General characterization information.

All tests were performed at room temperature unless otherwise noted. ^{1}H and ^{11}B NMR spectra were recorded on an Agilent 400 MHz spectrometer using $CDCl_3$ or DMSO-d_6 as solvent, background subtraction of the borosilicate NMR tube was made using solvents without samples. The chemical structures of the films were characterized using a Nicolet Nexus 67 Fourier transform infrared spectrophotometer with an attenuated total reflection assemble (FTIR-ATR, Thermo Scientific, USA). The spectra were obtained by examined the films for 32 scans with a resolution of 2 cm^{-1} in the 4000-500 cm^{-1} range. Thermo gravimetric analysis (TGA) measurement was performed on Q500 (TA Instrument, USA) with a heating rate of 10 °C min^{-1} from 40 to 700 °C under nitrogen atmosphere. Wide-angle X-ray diffraction (WAXD) measurements were

carried out on a Rigaku RU-200 diffractometer (Rigaku Co., Japan) using Ni-filtered Cu Ka radiation (λ =0.154 nm) at 20 °C. The instrument was worked at 40 kV and 200 mA. The sample was step-scanned from 10 to 40° at a 2θ scanning rate of 2 ° min^{-1}. Small-angle X-ray scattering (SAXS) measurements were carried out on Anton Paar SAXSpoint 2.0 (Anton Paar, Austria). The scattering pattern was recorded on an imaging plate (IP) with a pixel size of 75×75 μm^2 which extended to the high-angle range.

3.2 Tensile test.

Tensile tests were performed on SUNS UTM2502 instrument with 100 N load cell. For mechanical tensile-stress and self-healing test, sample size of 30 mm length × 4 mm width × 1 mm height, and strain rate of 100 mm min^{-1} were adopted. If not specified, cycle tensile tests were performed at a rate of 100 mm min^{-1}. Toughness of test specimens were calculated by the integration of the area under the stress-strain curves. The temperature and relative humidity for tensile tests was 25±1°C and 40±5%, respectively. The mechanical properties were obtained from the immediate measurement on samples being taken out from a dry desiccator to minimize the effect of environment moisture.

To investigate the effect of water on the mechanical properties, the specimens were exposed to different relative humidity of 55% (RH55) for a certain period of time before tensile test. The percentage of water in the sample was determined by weighting. The environment with relative humidity of 55% (RH55) was prepared using saturated aqueous sodium bromide solution in a sealed container at 25 °C.

3.3 Self-healing test.

Self-healing tests were evaluated mainly by scratch recovery and restoration of mechanical properties at room-temperature for various period of time. Scratch recovery tests were performed by scratching neat films with a razor blade. Scratches were crossed over another obliquely to easily track the changes of the scratch-width using an optical microscope. The scratch of the samples wetted or not with water. Restoration of

the mechanical properties was assessed by cutting the samples into two completely separate pieces with a razor blade and the damaged ends were dipped into water for 1 min or not. The two separated pieces were brought into contact for 2 min and the residual water was removed by drying at room temperature for different time durations to heal the damage. It is noted that the healing efficiency in this study was defined as the proportion of restored toughness to the original toughness on the account of the recovery of both stress and strain in the materials.

3.4 Calculation of the fracture energy.

In the Rivlin and Thomas method method[1], two different samples, notched and unnotched, were used to measure the tearing energy, E_f. Rectangular-shaped specimens (4mm in width× 30mm in length× 1.0mm in thickness) were used. An initial notch of 1mm in length was cut using a razor blade. According to the study of Suo[2] , the precise length of the notch was unimportant for this test. The specimen was clamped on two sides, and the distance between the two clamps was fixed at 5mm (L_0). **(Fig. S12a)** The under clamp was pulled at 100 mm min^{-1}, with the upper clamp fixed. The force-length curves of the samples were recorded, and the tearing energy was calculated using the following equation (Eq. S1):

$$E_f = \frac{U(Lc)}{a_o \times b_0} \qquad \text{(Eq. S1)}$$

where $U(Lc)$ is the work done by the applied force to the unnotched sample at the critical strectching distance Lc, and Lc is the distance between the two clamps when the crack starts to propagate in the notched sample. The plateau in the force-displacement curve of the notched sample suggests the propagation of the crack. Accordingly, Lc, as shown in **Fig S12b**, is defined as the critical displacement when the force plateau appears. The yellow colored-area corresponds to the work, $U(Lc)$, done by the applied force to the unnotched sample.

While in the Greensmith method[3] as shown in **Fig. S13**, the fracture energy G_c was calculated using the following equation (Eq. S2):

$$G_{\mathrm{C}} = \frac{6Wc}{\sqrt{\lambda_{\mathrm{c}}}} \qquad \text{(Eq. S2)}$$

Where c is the notch length; W is the strain energy calculated by integration of the stress-strain curve of an un-notched specimen until λ_{c}.

Since many reported fracture energies were calculated using the Greensmith method. For a better and clear comparison, the fracture energies for several self-healing elastomers and tough hydrogels in literature from above two methods are compared and graphically shown in **Fig. S14**.

3.5 Rheology measurement and time-temperature superposition (TTS).

Small amplitude oscillatory shear (SAOS) measurements were performed on a HAAKE RheoStress 600 instrument in the frequency range of 100-0.1 rad s^{-1} at 110, 100, 80, 60, and 40 ºC in the linear viscoelastic region of 1 %, respectively. Master curves at the reference temperature of 25 ºC were scaled by WLF equation.

$$\log\left(a_T\right) = \frac{-C_1\left(T - T_r\right)}{C_2 + \left(T - T_r\right)} \qquad \text{(Eq. S3)}$$

Where a_T the horizontal is shift factor, and T_r is the reference temperature.

The transient creep-recovery measurements were performed on a DHR-1 rotary rheometer (TA Instruments, USA) under the nitrogen atmosphere in parallel plates with diameters of 8 mm. The stress appled on the sample was 1500 Pa.

3.6 Computational Method.

The Gaussian09 suite of programmes[4] was used for the calculations in this study. The M06-2X[5] method combined with the 6-31G* basis set was used for unrestricted geometry optimization in a tetrahydrofuran solvent (consistent with the experiment, with the SMD[6] model) on all structures. To verify the stationary points to be local minima or saddle points, we conducted frequency analysis at the same level with optimization. The M06-2X/6-311++G** method with the SMD model was used for the solution phase single-point energy calculations of all of these stationary points. All

energetics involved in this study are the single point energy calculated at the M06-2X/6-311++G** method.

4. Supplementary Figures

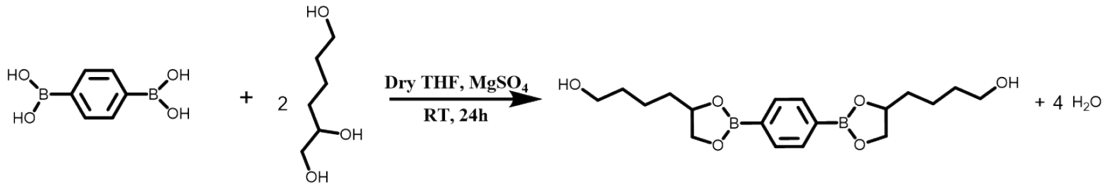

Fig. S1. Synthetic route of HDB.

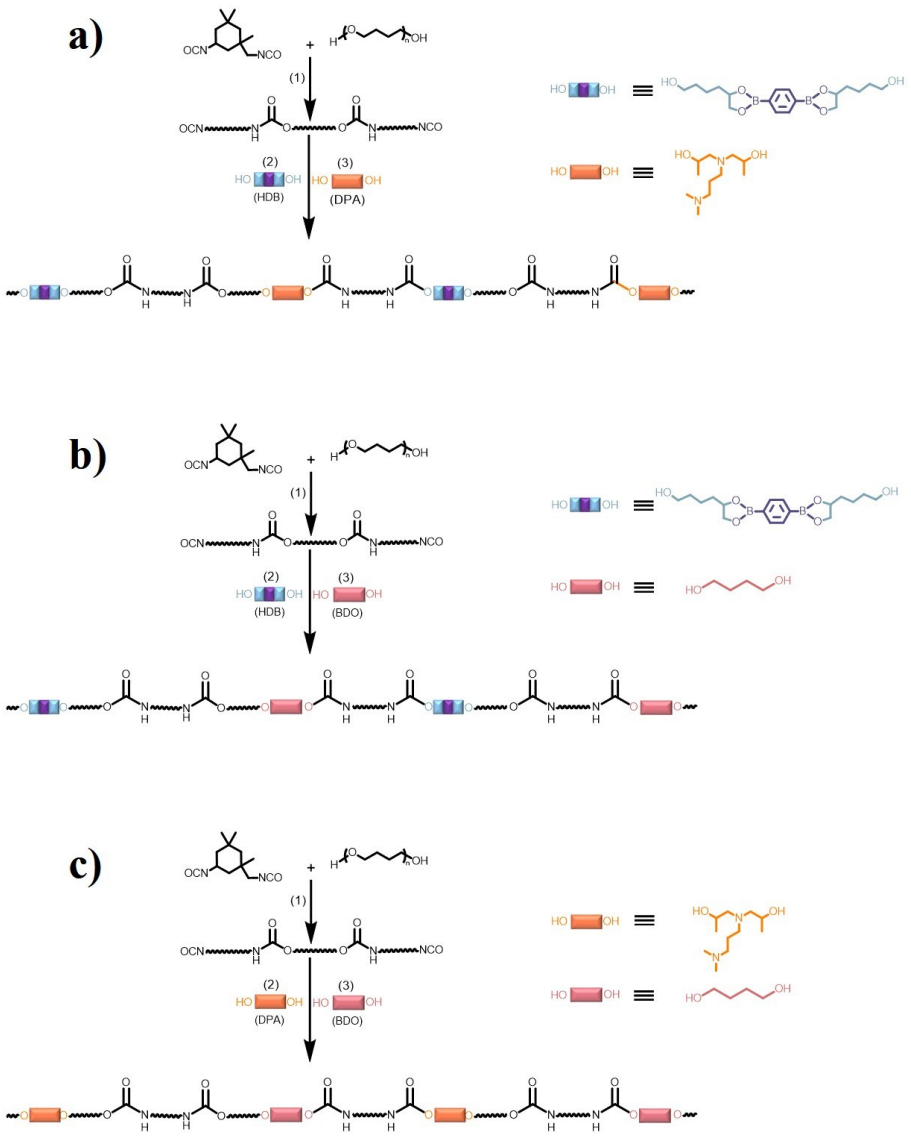

Fig. S2. Synthetic routes of (a) PU-BN_x, (b) PU-B_9 and (c) PU-B_0.

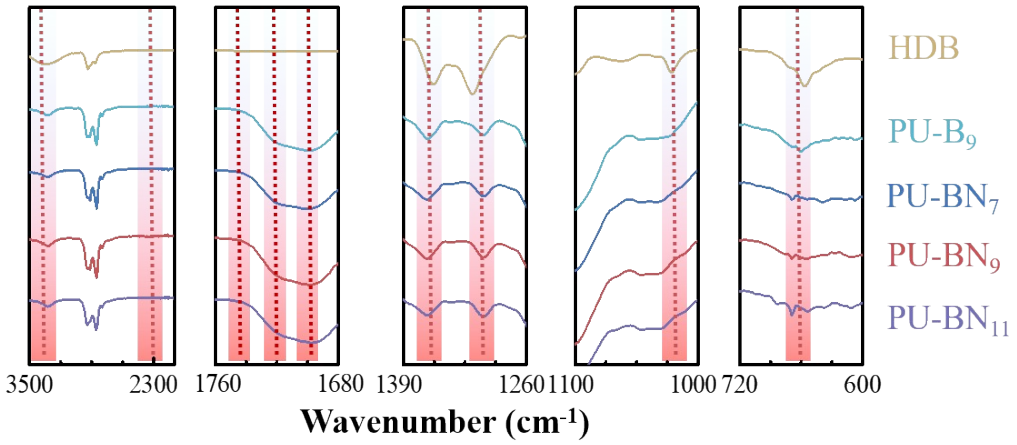

Fig. S3. ATR-FTIR spectra for HDB, PB-B_9, PU-BN_7, PU-BN_9, PU-BN_{11}.

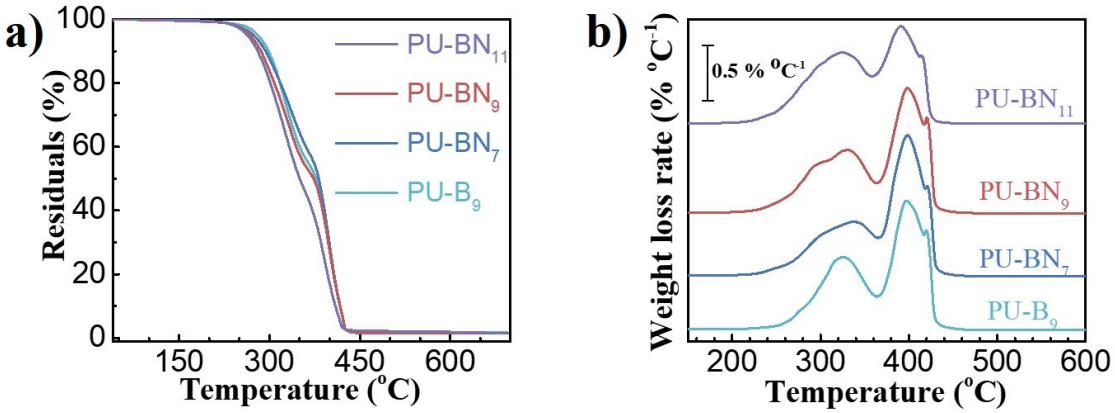

Fig. S4. TGA (a) and DTG (b) curves of PU-BN_7, PU-B_9, PU-BN_9 and PU-BN_{11}.

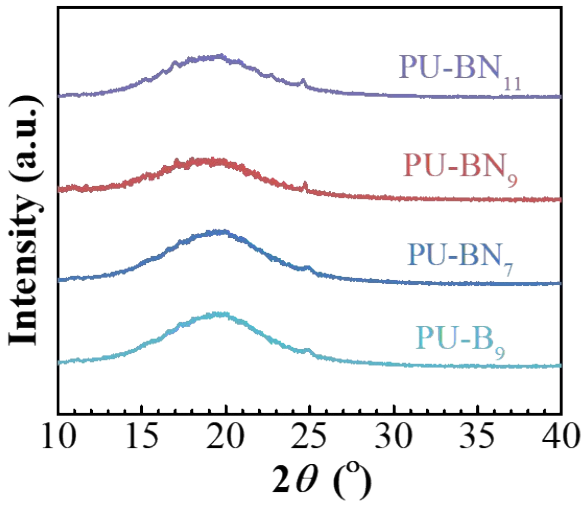

Fig. S5. XRD profiles of PU-BN_7, PU-B_9, PU-BN_9 and PU-BN_{11}.

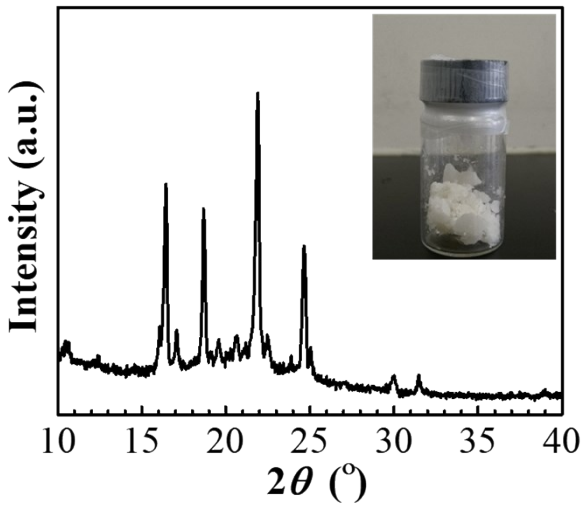

Fig. S6. XRD profile of HDB.

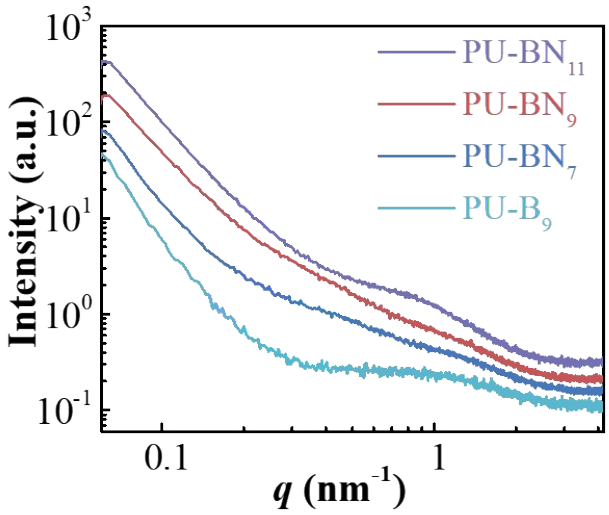

Fig. S7. SAXS patterns of PU-BN_7, PU-B_9, PU-BN_9 and PU-BN_{11}.

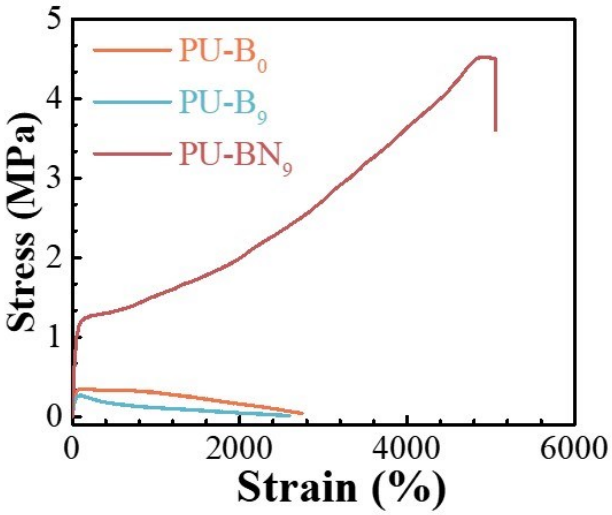

Fig. S8. Stress-strain curves of PU-B_0, PU-B_9 and PU-BN_9.

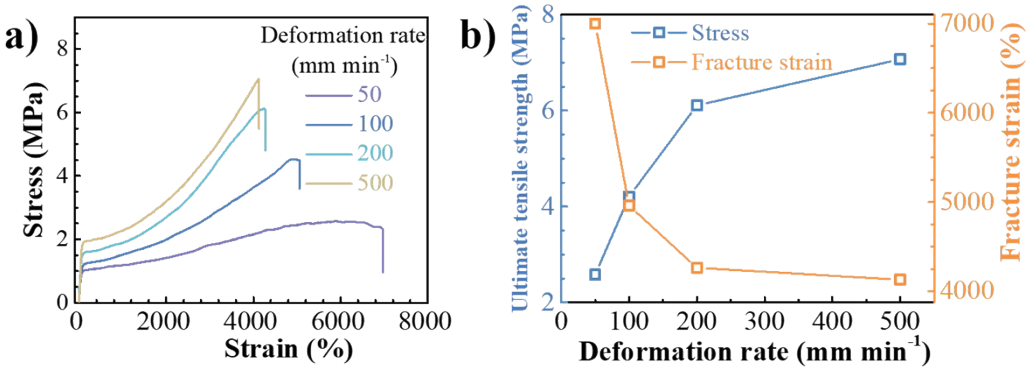

Fig. S9. (a) Stress-strain curves of PU-BN_9 under different deformation rates in the range of 50 to 500 mm min^{-1}. (b) Deformation rate dependence of PU-BN_9 on the ultimate tensile strength and fracture strain.

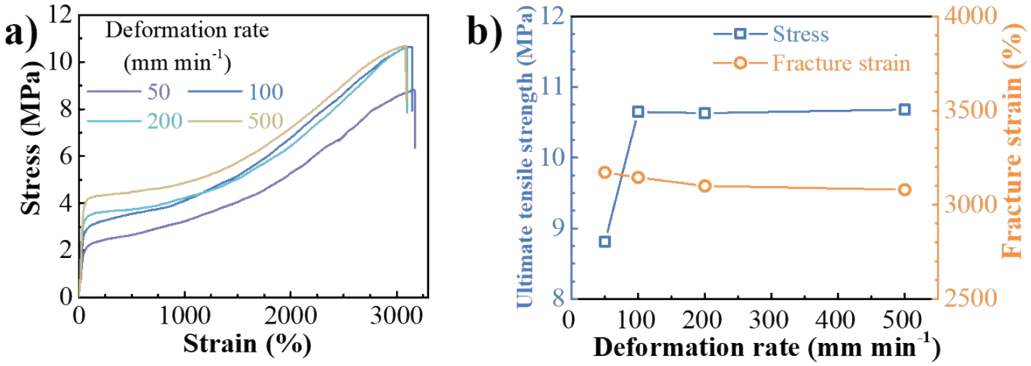

Fig. S10. (a) Stress-strain curves of PU-BN_{11} under different deformation rates in the range of 50 to 500 mm min^{-1}. (b) Deformation rate dependence of PU-BN_{11} on the ultimate tensile strength and fracture strain.

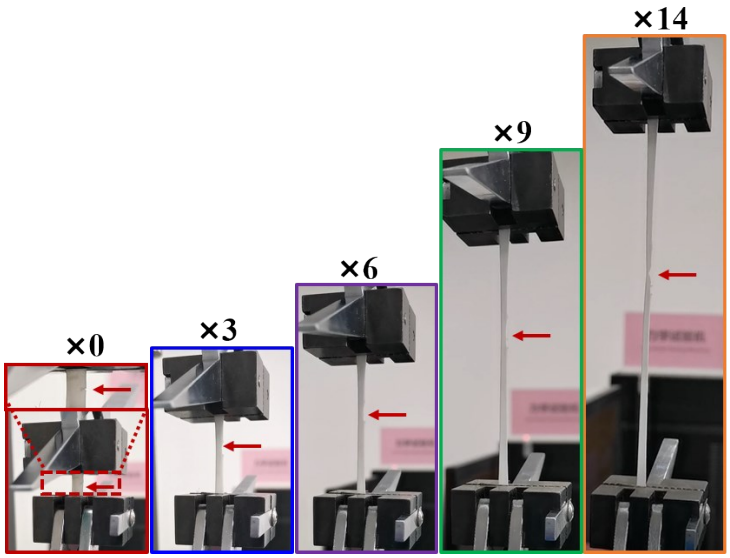

Fig. S11. A notched PU-BN_9 film before stretching and after 300%, 600%, 900% and 1400% stretching, demonstrating that the film is notch insensitive.

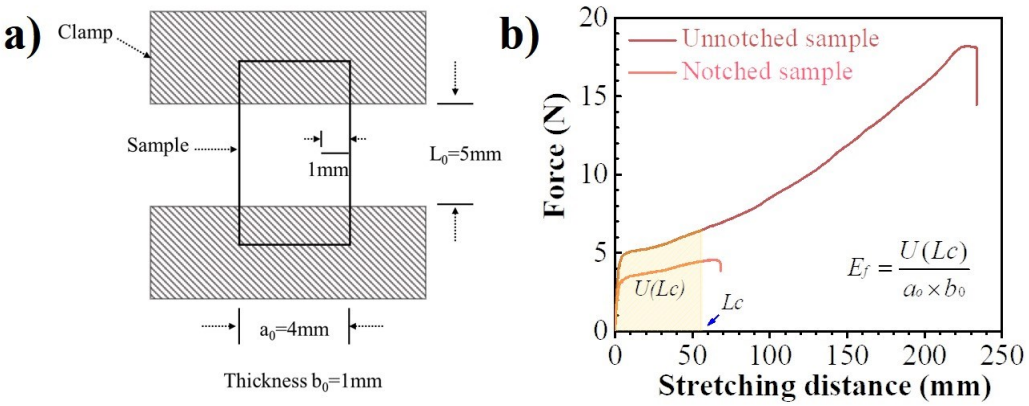

Fig. S12. a) Schematic illustration of the single-edge-notched sample used for the pure shear test for the determination of the fracture energy of the sample. b) Force-displacement curves of the unnotched and single-edge-notched PU-BN_9 samples with the same dimension to illustrate the Rivlin and Thomas method to determine the fracture energy. The plateau in the force-displacement curve of the notched sample suggests the propagation of the crack. Accordingly, L_c, as shown in the figure, is defined as the critical displacement when the crack in the notched sample starts to propagate.

The yellow colored area in the figure corresponds to the work $U(L_c)$ done by the applied force to the unnotched sample.

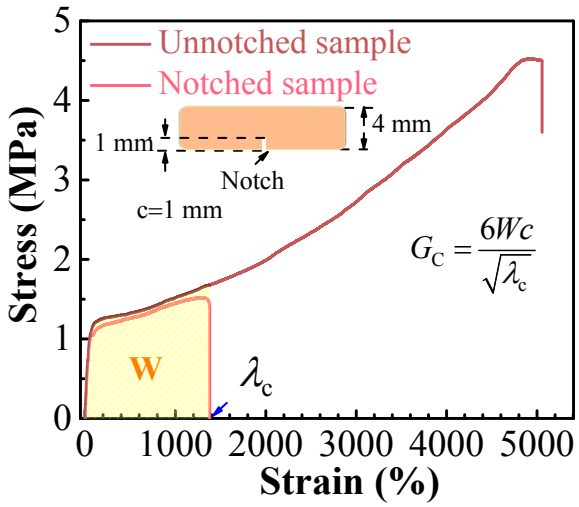

Fig. S13. Illustration of the Greensmith method to determine fracture energy from Stress-strain curves, using PU-BN_9 as the example.

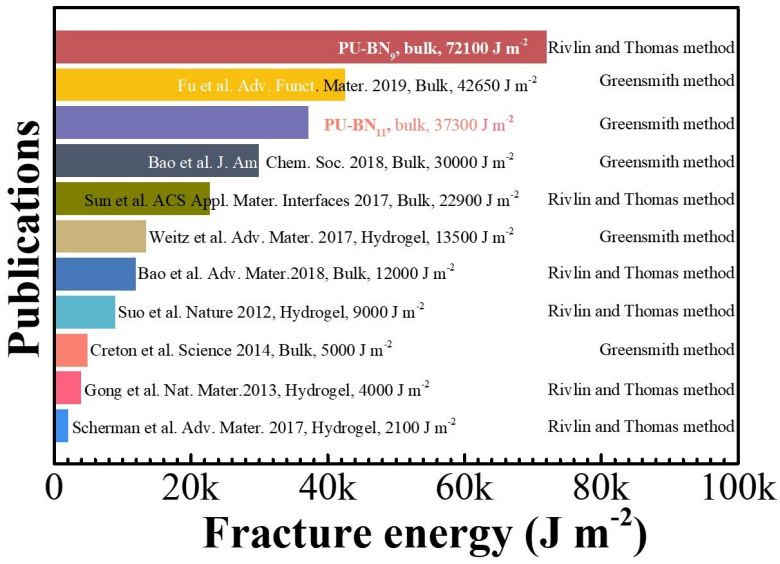

Fig. S14. Graphic comparison of the fracture energies for some classical stretchable polymer elastomers and tough hydrogels, which were calculated using the Greensmith method and Rivlin and Thomas method as indicated.

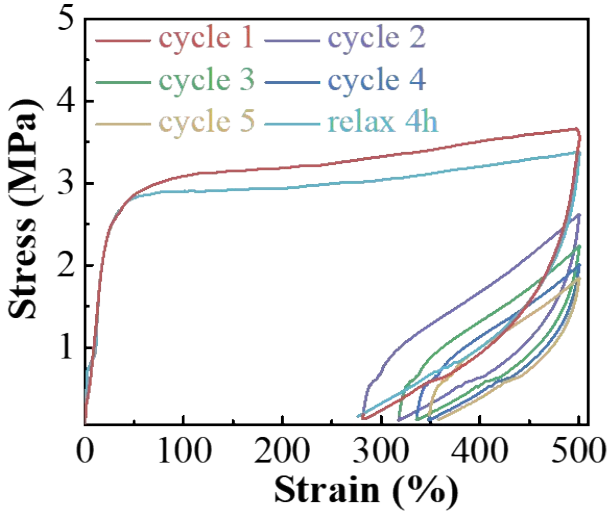

Fig. S15. (a) Repeated cyclic tensile curves of PU-BN_{11} at 500%.

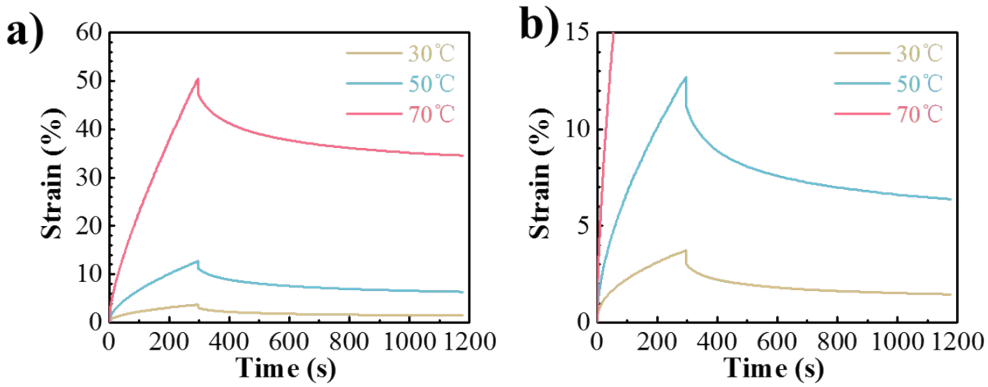

Fig. S16. (a) Creep and recovery of PU-BN_{11} at 30, 50, and 70 °C at a constant stress of 1500 Pa. (b) Enlarged (a) at small strain. The sample experienced creep when applied an external stress of 1500 Pa and the crept strain after 300 s increased with temperature from 4% at 30 °C to 51 % at 70 °C. After removal of the applied stress, the sample can recover 61% and 32 % of its strain at 30 and 70 °C, respectively, indicating that less irreversible deformation had occurred at lower temperature.

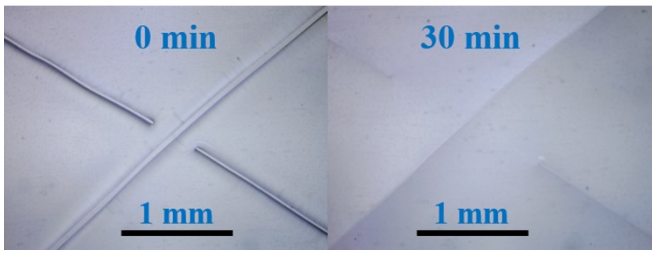

Fig. S17. Optical microscopy images of the X-shaped scratch on PU-BN_7 films without the aid of water.

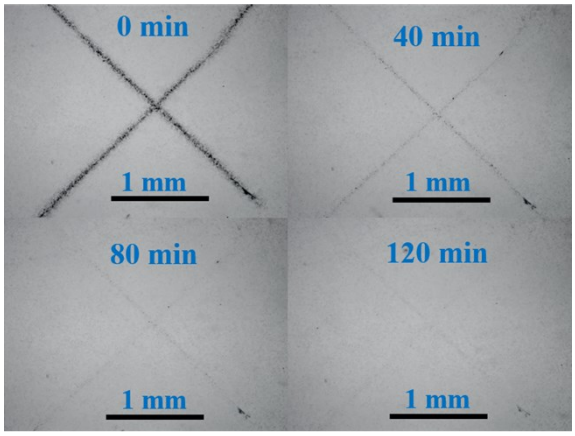

Fig. S18. Optical microscopy images of the X-shaped scratch on PU-BN_9 films without the aid of water.

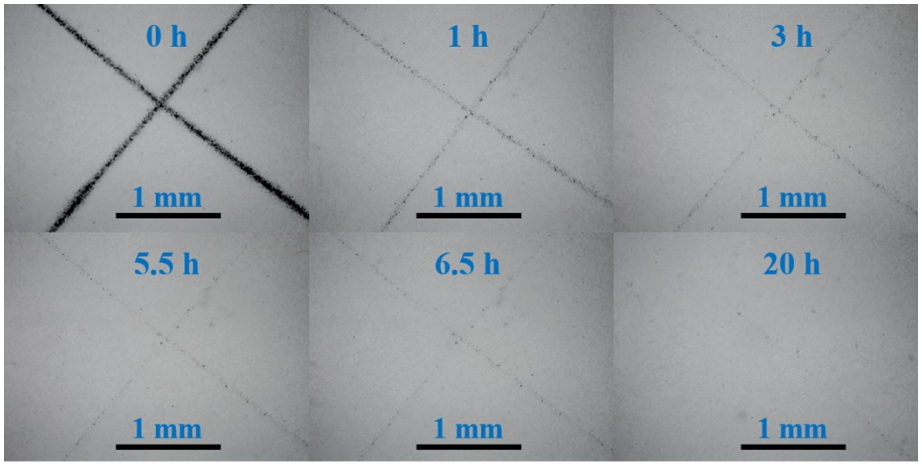

Fig. S19. Optical microscopy images of the X-shaped scratch on PU-BN_{11} films without the aid of water.

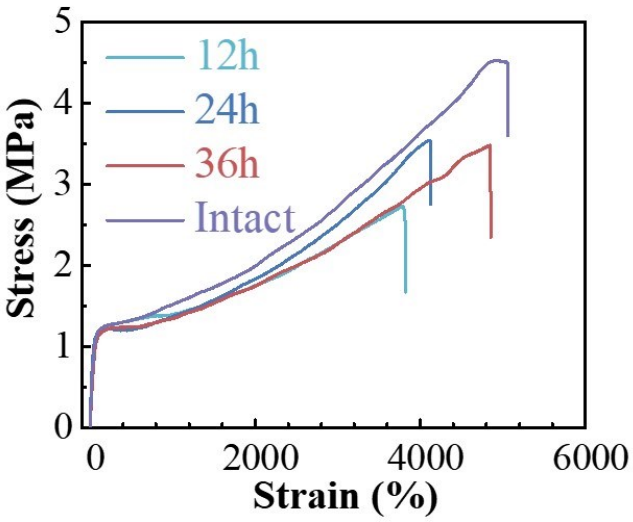

Fig. S20. Typical stress-strain curves of original and self-healed PU-BN_9 at room temperature for different time without the aid of water.

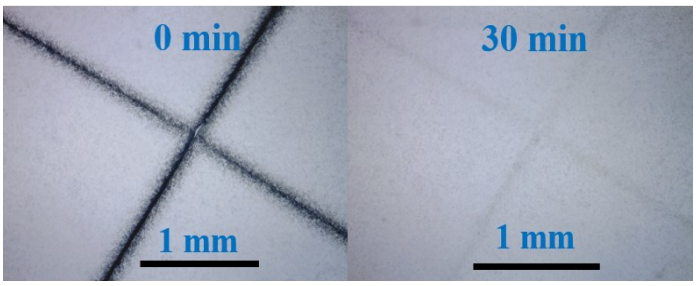

Fig. S21. Optical microscopy images of the X-shaped scratch on PU-BN_9 films with the aid of water.

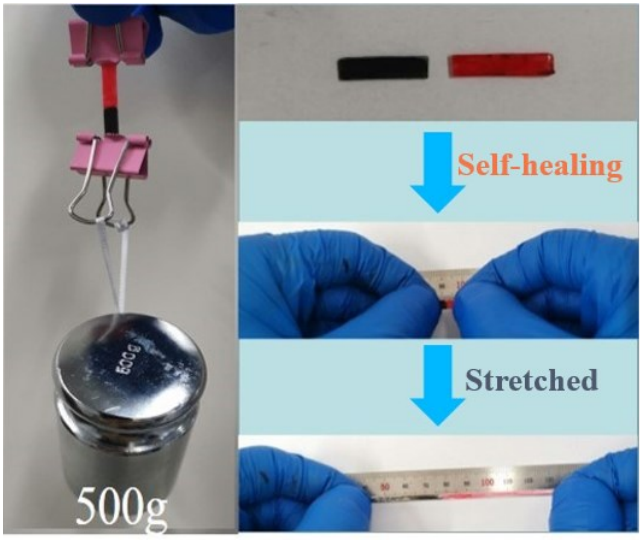

Fig. S22. Photographs of the bulky self-healing process of PU-BN_{11}.

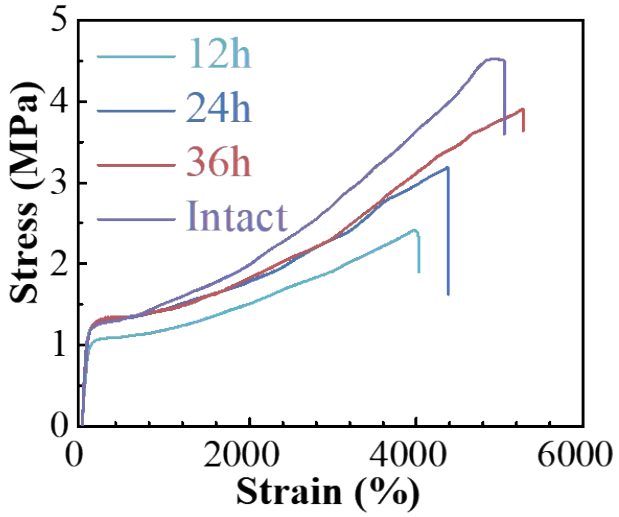

Fig. S23. Typical stress-strain curves of original and self-healed PU-BN_9 at room temperature for different time with the aid of water.

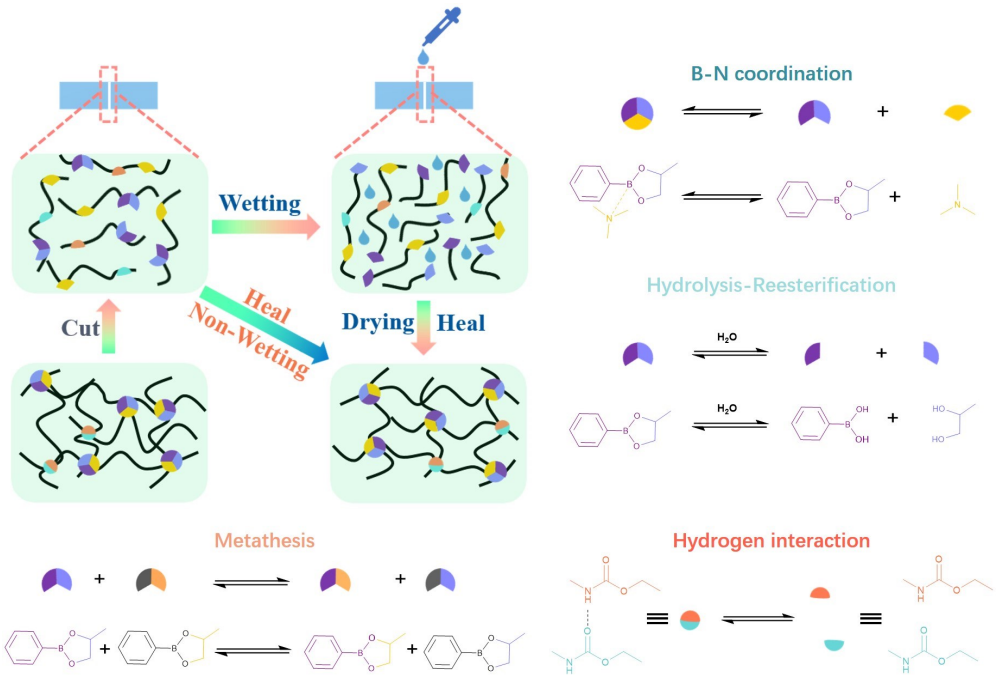

Fig. S24. Proposed mechanism of healing with and without the aid of water. Quadruple dynamic mechanisms including metathesis, hydrolysis-reesterification, B-N coordination, and hydrogen interaction.

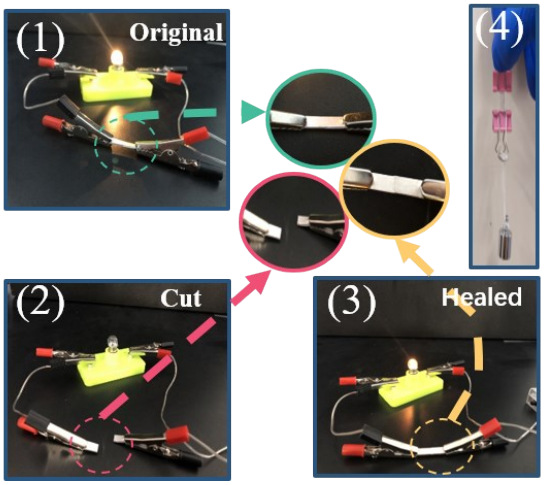

Fig. S25. Demonstration of the self-healing properties for the composite conductor. The lamp was lit at the original stage (1) and turned off after the conductor being cut (2). The severed composite conductor was efficiently healed with the aid of water. The lamp turned back on after healing (3). The healed conductor can hold a weight of 50g (4).

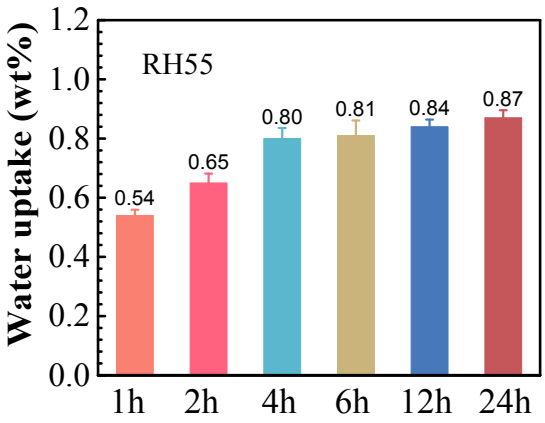

Fig. S26. Water uptake of PU-BN11 after different time of exposure in a chamber of RH55.

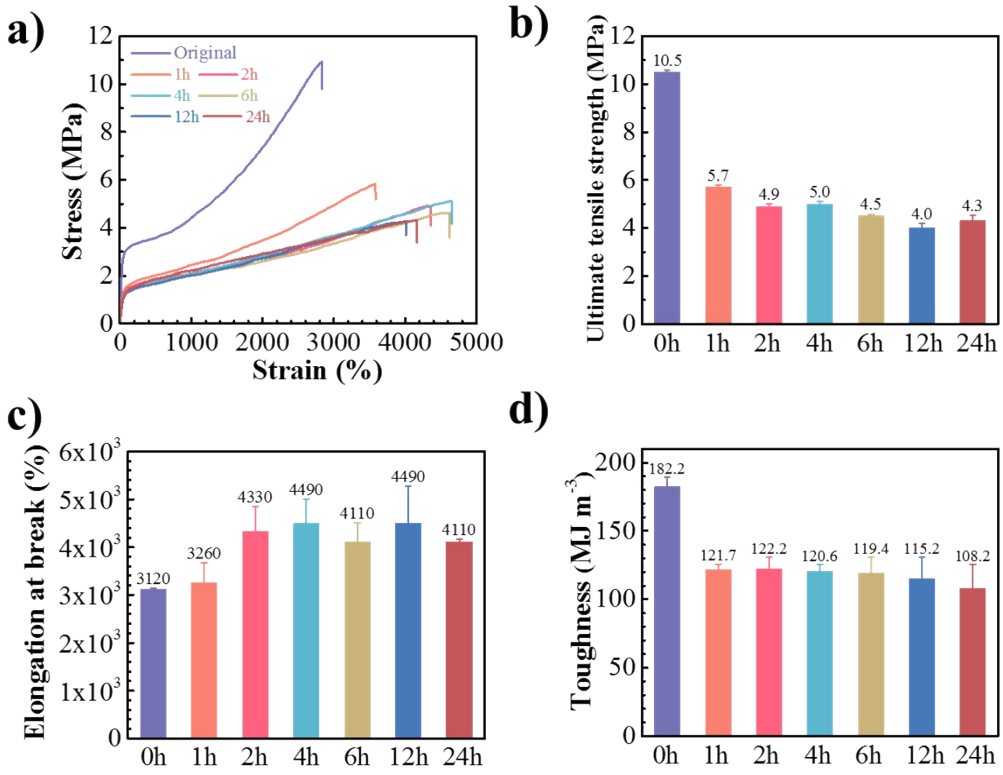

Fig. S27. Mechanical properties of PU-BN_{11} after different time of exposure in a chamber of RH55: (a) stress-strain curves, (b) ultimate tensile strength, (c) elongation at break, (d) tensile toughness. PU-BN_{11} exhibited remarkable decrease on the ultimate tensile strength by 59%, as compared to dry PU-BN_{11} after exposure for 24 h. On the

contrary, the elongation at break experienced increase sufficiently. The tensile toughness that accounts both stress and strain consequently exhibited a similar decline with a lower rate and only 41% of decrease was observed after 24h. The water absorbed in the sample could lead to hydrolysis of boronic esters and breakage of the hydrogen bonds and B-N coordination, which deteriorated the mechanical properties seriously.

5. Tables

Table S1. Formulations of PU-B_0, PU-B_9, and PU-BN_x.

Sample	Molar ratio (IPDI/PTMEG/HDB/BDO/DPA)	HDB content (wt %)
PU-B_0	12.5/5.0/0.0/5.0/2.5	0.00
PU-B_9	12.5/5.0/2.5/5.0/0.0	9.91
PU-BN_7	12.0/6.0/2.0/0.0/4.0	7.06
PU-BN_9	12.5/5.0/2.5/0.0/5.0	9.26
PU-BN_{11}	13.5/4.5/3.0/0.0/6.0	10.98

Table S2. The bond length of B-O in HDB, B-N1, B-N2 and electronic energy of eq1 (B-N1) and eq2 (B-N2).

	B-O (Å)	B-O (Å)	B-N (Å)	ΔE (kcal mol^{-1})
HDB	1.369	1.369		
HDB-N1 (B-N1)	1.451	1.451	1.707	-13.98
HDB-N2 (B-N2)	1.451	1.451	1.754	1.16

Table S3. Parameters of $PU\text{-}B_9$, $PU\text{-}BN_9$, and $PU\text{-}BN_{11}$.

Sample	ω_0 (rad s^{-1})	τ_d (s)
$PU\text{-}BN_9$	0.21	4.8
$PU\text{-}B_9$	0.0013	769.2
$PU\text{-}BN_{11}$	0.0012	833.3

Table S4. Mechanical properties of $PU\text{-}B_0$, $PU\text{-}B_9$, and $PU\text{-}BN_x$.

Sample	Yield strength (MPa)	Young's modulus (MPa)	Ultimate tensile strength (MPa)	Elongation at break (%)	Tensile toughness (MJ m^{-3})
$PU\text{-}B_0$	0.35±0.1	1.7±0.1	0.35±0.1	2740±70	5.7±0.3
$PU\text{-}B_9$	0.3±0.1	0.7±0.1	0.3±0.1	2590±45	2.6±0.1
$PU\text{-}BN_7$	0.6±0.1	1.4±0.3	0.7±0.1	14050±1150	54.7±1.2
$PU\text{-}BN_9$	1.2±0.1	3.1±0.5	4.2±0.3	4960±100	119.8±9.6
$PU\text{-}BN_{11}$	2.8±0.1	8.6±0.1	10.5±0.1	3120±20	182.2±7.1

Table S5. Estimated ultimate tensile strength, elongation at break, toughness, and recovery tests of various self-healing polymers at room temperature.

Self-healing motif	Virgin			Time for self-healing (h)	Healed			Refs
	Ultimate tensile strength (MPa)	Elongation at break (%)	Toughness (MJ m^{-3})		Ultimate tensile strength (MPa)	Elongation at break (%)	Toughness (MJ m^{-3})	
Boronic ester	**10.5**	**3120**	**182.2**	**36**	**8.6**	**2630**	**123.5**	**This study**
	4.4	58	1.4	72	4.0	53	1.2	[7]
	2.1	450	6.0	72	1.7	490	5.7	[8]
	2.9	542	10.1	16 (50 oC)	2.9	523	9.2	[9]
Disulfides	6.8	923	26.9	2	6.0	920	20.6	[10]
	4.3	128	3.1	48	3.7	113	2.6	[11]
Acylhydrazone	0.3	11700	14.1	24	0.25	10650	10.7	[12]
van der Waals	4.4	560	12.0	120	4.4	500	11	[13]
Hydrogen bonding	6.3	852	23.2	24	6.3	847	22.9	[14]
	1.9	780	10.0	24	1.7	710	8	[15]
	1.7	1735	14.9	48	1.3	1583	10.9	[16]
	1.9	1508	17.6	24	1.8	1460	16.3	[17]
Diselenide	2.1	700	6.6	24	1.6	620	4.5	[18]
Metal-ligand	1.5	780	9.9	3	1.5	760	9.8	[19]
	3.2	1071	29.3	12	3.2	1050	25.1	[20]
oxime	14.8	1210	87.0	130	13.8	1080	78.3	[21]
ionic interactions	10.3	366	29.0	3	8.4	454	24	[22]
	5.2	1667	40.1	44	4.9	1665	35.3	[23]
Boroxine	12.7	184	17.5	18	11.7	172	15.8	[24]

6. Movies.

Movie S1. This movie shows the ultra-high extensibility of PU-BN_7 film.

Movie S2. This movie shows the outstanding notch insensitiveness of PU-BN_9 film.

Movie S3. This movie shows the excellent puncture resistance of PU-BN_{11} film.

7. References.

[1] R. S. Rivlin, A. G. Thomas, *Journal of Polymer Science* 1953, ***10***, 291-318.

[2] J. Y. Sun, X. Zhao, W. R. Illeperuma, O. Chaudhuri, K. H. Oh, D. J. Mooney, J. J. Vlassak, Z. Suo, *Nature* 2012, ***489***, 133-136.

[3] H. W. Greensmith, *J. Appl. Polym. Sci.* 1963, ***7***, 993-1002.

[4] J. R. S. Cheeseman, G.; Barone, V.; Mennucci, B.; Petersson, G. A.; Nakatsuji, H.; Caricato, M.; Li, X.; Hratchian, H. P.; Izmaylov, A. F.; Bloino, J.; Zheng, G.; Sonnenberg, J. L.; Hada, M.; Ehara, M.; Toyota, K.; Fukuda, R.; Hasegawa, J.; Ishida, M.; Nakajima, T.; Honda, Y.; Kitao, O.; Nakai, H.; Vreven, T.; Montgomery, J. A., Jr; Peralta, J. E.; Ogliaro, F.; Bearpark, M.; Heyd, J. J.; Brothers, E.; Kudin, K. N.; Staroverov, V. N.; Keith, T.; Kobayashi, R.; Normand, J.; Raghavachari, K.; Rendell, A.; Burant, J. C.; Iyengar, S. S.; Tomasi, J.; Cossi, M.; Rega, N.; Millam, J. M.; Klene, M.; Knox, J. E.; Cross, J. B.; Bakken, V.; Adamo, C.; Jaramillo, J.; Gomperts, R.; Stratmann, R. E.; Yazyev, O.; Austin, A. J.; Cammi, R.; Pomelli, C.; Ochterski, J. W.; Martin, R. L.; Morokuma, K.; Zakrzewski, V. G.; Voth, G. A.; Salvador, P.; Dannenberg, J. J.; Dapprich, S.; Daniels, A. D.; Farkas, O.; Foresman, J. B.; Ortiz, J. V.; Cioslowski, J.; Fox, D. J., *Gaussian 09, revision D.01; Gaussian, Inc.: Wallingford, CT* 2013.

[5] Y. Zhao, D. G. Truhlar, *Theor. Chem. Acc.* 2008, ***120***, 215-241.

[6] A. Höllwarth, M. Böhme, S. Dapprich, A. W. Ehlers, A. Gobbi, V. Jonas, K. F. Köhler, R. Stegmann, A. Veldkamp, G. Frenking, *Chem. Phys. Lett.* 1993, ***208***, 237-240.

[7] J. J. Cash, T. Kubo, A. P. Bapat, B. S. Sumerlin, *Macromolecules* 2015, ***48***, 2098-2016.

[8] C. Kim, H. Ejima, N. Yoshie, *J. Mater. Chem. A* 2018, ***6***, 19643-19652.

[9] O. R. Cromwell, J. Chung, Z. Guan, *J. Am. Chem. Soc.* 2015, ***137***, 6492-6495.

[10] S. M. Kim, H. Jeon, S. H. Shin, S. A. Park, J. Jegal, S. Y. Hwang, D. X. Oh, J. Park, *Adv. Mater.* 2018, ***30***, 1705145-n/a.

[11] R. H. Aguirresarobe, L. Martin, M. J. Fernandez-Berridi, L. Irusta, *Express Polym. Lett.* 2017, ***11***, 266-277.

[12] P. Wang, G. Deng, L. Zhou, Z. Li, Y. Chen, *ACS Macro. Lett.* 2017, ***6***, 881-886.

[13] A. Susa, R. K. Bose, A. M. Grande, S. van der Zwaag, S. J. Garcia, *ACS Appl. Mater. Interfaces* 2016, ***8***, 34068-34079.

[14] Y. Wang, X. Liu, S. Li, T. Li, Y. Song, Z. Li, W. Zhang, J. Sun, *ACS Appl Mater Interfaces* 2017, ***9***, 29120-29129.

[15] Y. Chen, A. M. Kushner, G. A. Williams, Z. Guan, *Nat. Chem.* 2012, ***4***, 467-472.

[16] J. Kang, D. Son, G. N. Wang, Y. Liu, J. Lopez, Y. Kim, J. Y. Oh, T. Katsumata, J. Mun, Y. Lee, L. Jin, J. B. Tok, Z. Bao, *Adv. Mater.* 2018, ***30***, e1706846.

[17] Y. Pan, J. Hu, Z. Yang, L. Tan, *ACS Appl. Polym. Mater.* 2019, ***1***, 425-436.

[18] X. An, R. H. Aguirresarobe, L. Irusta, F. Ruipérez, J. M. Matxain, X. Pan, N. Aramburu, D. Mecerreyes, H. Sardon, J. Zhu, *Polym. Chem.* 2017, ***8***, 3641-3646.

[19] D. Mozhdehi, S. Ayala, O. R. Cromwell, Z. Guan, *J. Am. Chem. Soc.* 2014, ***136***, 16128-16131.

[20] J. C. Lai, X. Y. Jia, D. P. Wang, Y. B. Deng, P. Zheng, C. H. Li, J. L. Zuo, Z. Bao, *Nat. Commun.* 2019, ***10***, 1164.

[21] L. Zhang, Z. Liu, X. Wu, Q. Guan, S. Chen, L. Sun, Y. Guo, S. Wang, J. Song, E. M. Jeffries, C. He, F. L. Qing, X. Bao, Z. You, *Adv. Mater.* 2019, ***31***, 1901402.

[22] J. Zhang, M. Huo, M. Li, T. Li, N. Li, J. Zhou, J. Jiang, *Polymer* 2018, ***134***, 35-43.

[23] Y. Miwa, J. Kurachi, Y. Kohbara, S. Kutsumizu, *Commun. Chem.* 2018, ***1***, 5.

[24] C. Bao, Y.-J. Jiang, H. Zhang, X. Lu, J. Sun, *Adv. Funct. Mater.* 2018, ***28***, 1800560.